

Maximal spreading of impacting viscoelastic droplets

Orr Avni,* Dongyue Wang,* and Roberto Zenit†

*School of Engineering, Brown University,
184 Hope Street, Providence, RI 02912, USA*

Mithun Ravisankar

*Department of Mathematics, Mechanics division,
University of Oslo, Oslo 0316, Norway*

(Dated: January 22, 2026)

Abstract

Droplet impact and spreading on solid substrates are well understood for Newtonian fluids, yet how viscoelasticity alone modifies the maximal spreading remains unclear. To discern the physical mechanisms governing the spreading dynamics, we present a simplified theoretical model, validated by impact experiments, to quantify how fluid elasticity modifies the maximal spreading of impacting droplets. Experiments were performed using fluids within a narrow range of viscosity and surface tension, but varying relaxation time. While following similar asymptotic scalings as Newtonian droplets, the maximum diameter for viscoelastic droplets exhibits a clear deviation from Newtonian behaviour only when the Deborah number is of order unity. The maximum spread diameter is reduced by as much as 40% from the expected value for Newtonian fluid. These results support the central prediction of our model: an extension of classical energy balance that incorporates viscoelastic effects through a single correction factor. The model captures the observed reduction in maximal spreading and predicts both the location and magnitude of the most substantial viscoelastic effects, providing a basis for extending impact models beyond purely Newtonian fluids.

* These authors contributed equally to this work

† roberto_zenit@brown.edu

I. INTRODUCTION

Droplet impact on solid substrates is a canonical problem in fluid mechanics; it is a critical aspect in many engineering applications, ranging from inkjet printing and additive manufacturing to agricultural spraying and thermal control [1–3]. Despite its apparent simplicity, the impact event couples inertia, viscosity and capillary effects over a broad range of time and length scales. This leads to complex dynamics and outcomes, including spreading, recoiling, bouncing and splashing [4–6]. For Newtonian liquids, extensive theoretical, numerical and experimental work has established how the maximal spreading diameter D_{\max} depends on the impact conditions, i.e. the droplet initial size D_0 and impact velocity U_0 , as well as the fluid properties. These are commonly expressed in terms of the impact Weber, Reynolds and Ohnesorge numbers, $\text{We} = \rho U_0^2 D_0 / \sigma$, $\text{Re} = \rho U_0 D_0 / \mu$, and $\text{Oh} = \sqrt{\text{We}} / \text{Re} = \mu / \sqrt{\rho \sigma D_0}$, respectively [6–10].

Numerous scaling arguments predict two principal asymptotic regimes: viscous-limited and capillary-limited spreading. In the viscous regime, where $\text{We} \gg \text{Re}^{1/2}$, scaling arguments suggest that the maximal diameter scales as either $\text{Re}^{1/4}$ or $\text{Re}^{1/5}$ [7, 8]. In the capillary regime, energy-conservation considerations demand $\bar{D}_{\max} \sim \text{We}^{1/2}$, whereas a momentum-balance argument yields $\bar{D}_{\max} \sim \text{We}^{1/4}$. Laan *et al.* [11] proposed a semi-empirical approximation that bridges these limiting cases by introducing the impact parameter $P = \text{Re}^{-2/5} \text{We}$ and the Padé-type correlation

$$\bar{D}_{\max} \text{Re}^{-1/5} = \frac{\sqrt{P}}{1.24 + \sqrt{P}}, \quad (1)$$

where $\bar{D}_{\max} = D_{\max} / D_0$. More recently, Sanjay and Lohse [9] reformulated the energy balance in terms of distinct impact and spreading stages, yielding a unified description of D_{\max} across a wide range of impact conditions and clarifying the role of viscous dissipation on the spreading process.

In contrast to Newtonian fluids, the effect of non-Newtonian rheology on impact spreading is less understood. On the one hand, several studies have demonstrated that the spreading diameter of such droplets can deviate from Newtonian scalings [12, 13]. Most recently, Mobaseri *et al.* [14] showed that existing Newtonian correlations may be extended to incorporate shear-thinning and shear-thickening drops by using an effective shear rate to account

for the average viscosity during spreading.

On the other hand, less is known about how viscoelasticity modifies the maximal spreading. Viscoelastic stresses are known to strongly affect free-surface flows and capillary thinning [15–17], and to alter the oscillations of free droplets [18]. Fluid elasticity in this context is usually quantified using the Deborah number, $De = \lambda/\tau$, defined as the ratio of the fluid elastic relaxation time λ to a characteristic flow timescale τ . Some studies report that, at large Deborah numbers $De > 10$, the spreading of non-Newtonian droplets is similar to that of Newtonian fluids [11, 19], whereas others find deviations from Newtonian behaviour during retraction [20, 21]. Yet, studies that systematically relate impact conditions and viscoelastic fluid properties to the maximal spreading over a wide range of parameters remain scarce.

Thus, the aim of this work is to quantify how fluid elasticity modifies the maximal spreading of impacting droplets and to identify the control parameters governing the departure of such fluids from Newtonian behaviour. We first introduce an extension of existing energy-balance models that incorporates viscoelastic effects. A description of an experimental apparatus follows, designed to test the impact of Newtonian and viscoelastic fluids within a narrow range of viscosity and surface tension, but varying relaxation time on glass and paper substrates. Finally, we compare the measured maximal spreading to both Newtonian correlations and our simplified viscoelastic model, uncovering the regime in which elasticity leads to a measurable reduction in spreading diameter.

II. SIMPLIFIED MODEL FOR PREDICTING VISCOELASTICITY EFFECTS

As a first step towards quantifying viscoelastic corrections, we consider an energy balance [9, 22]:

$$E_0 = \Delta E_\sigma + \Delta E_\mu + \Delta E_\lambda, \quad (2)$$

where E_0 is the initial kinetic energy, ΔE_σ is the change in surface energy, and ΔE_μ is the overall energy lost by viscous dissipation; we assume that no kinetic energy remains at maximal spread. The term for elastic energy stored in the fluid, dictating the extent to which viscoelasticity alters the spreading event, is

$$\Delta E_\lambda = V_\mu G \gamma^2, \quad (3)$$

where V_μ is the sheared liquid volume, γ is the radial strain, and G is the fluid's time-dependent elastic modulus. Assuming a Maxwell fluid, G may be expressed in terms of the spreading time τ_f as [17]

$$G(\tau_f) = \frac{\mu}{\tau_f \text{De}} \exp\left(-\frac{1}{\text{De}}\right), \quad (4)$$

where $\text{De} = \lambda/\tau_f$ is the Deborah number evaluated using the physical spreading time, and $\lambda = G_0/\mu$ is the fluid elastic relaxation time. Assuming the shear strain rate $\dot{\gamma}$ is constant throughout the expansion period, the elastic term may be combined with the viscous dissipation term to yield

$$\Delta E_\mu + \Delta E_\lambda = \mu V_\mu \tau_f \left(\frac{U_0}{\delta}\right)^2 \left(1 + \frac{1}{\text{De}} e^{-1/\text{De}}\right), \quad (5)$$

where δ is the viscous boundary-layer thickness [1]. Now, the viscoelastic effects are encapsulated within the term

$$\alpha = \frac{1}{\text{De}} \exp\left(-\frac{1}{\text{De}}\right). \quad (6)$$

The energy balance is further simplified by taking $\tau_f \approx \tau_0 = D_0/U_0$ and $\delta \approx D_0 \text{Re}^{-0.5}$, obtained from a similarity solution for boundary-layer flow [7]. Substituting these relations into equation (2), a simplified expression predicting the maximal spreading emerges as

$$\bar{D}_{max} = \sqrt{\frac{\text{We} + 12}{3(1 - \cos \theta_d) + 4(1 + \alpha) \text{We} \text{Re}^{-0.5}}}, \quad (7)$$

where $\bar{D}_{max} = D_{max}/D_0$ is the normalised maximal diameter and θ_d is the dynamic contact angle between the fluid and the substrate. In fact, equation (7) is an extension of the relation suggested by Pasandideh-Fard *et al.* [7]. For $\alpha = 0$ is similar in essence to other predictions proposed in recent literature [9, 14]. Equation (7), therefore, predicts how viscoelasticity, through $\alpha(\text{De})$, should modify the maximal spread relative to the Newtonian case; henceforth, we describe the experimental procedure used to measure \bar{D} and the associated fluid properties.

TABLE I. Properties of the test fluids.

Paper	Glass	Polymer	Glycerin	μ (mPas)	ρ (kg/m ³)	σ (mN/m)	λ (ms)
<i>Viscoelastic fluid set</i>							
●	○	6 ppm	80%	38.5	1193.4	77.3	4.6
▼	▽	25 ppm	50%	5.13	1121.4	69.7	5.7
■	□	30 ppm	50%	5.51	1131.2	71.6	8.0
◆	◇	50 ppm	0%	1.39	999.5	71.7	17.2
*		100 ppm	0%	1.68	997.2	73.8	61.9
★		150 ppm	0%	1.60	997.6	73.1	70.3
▲		200 ppm	0%	1.84	992.6	73.2	83.6
►		300 ppm	0%	1.92	996.8	73.0	79.7
<i>Newtonian set</i>							
×	+	0 ppm	80%	40.5	1199.6	77.3	0
×		0 ppm	30%	2.37	1064.2	71.6	0
	+	0 ppm	0%	1.05	998.4	71.2	0

III. EXPERIMENTAL SET-UP AND METHODS

To test the predictions of equation (7) and isolate the role of viscoelasticity, a set of different liquids with varying viscoelastic properties was prepared. First, stock aqueous solutions of non-ionic polyacrylamide polymer (PAAmm, Sigma Aldrich) with molecular weight $M_w = 5 \times 10^6$ g/mol were mixed; then, they were diluted with varying mixtures of glycerol (Nature's Oil, Vegetable Glycerin) and deionised water. The solutions were gently mixed using an overhead mixer for at least 12 hours to achieve homogeneity. To minimise viscosity shear-dependence, a small amount of magnesium sulfate salt (0.025 mol/l) was added to all solutions. The shear viscosity, density and surface tension of the fluids were measured using an ARES-G2 rheometer (TA Instruments), density meter (Anton Paar) and bubble pressure tensiometer (KRUSS Scientific Instruments), respectively. The relaxation time, λ , was determined using an in-house dripping-onto-substrate method, following previous works [23, 24]. To avoid polymer–polymer chain interaction and major variations in the zero-shear viscosity, the polymer concentration was kept below 300 ppm [24]. The shear-thinning observed in the dilute regime has a power index of $n \leq 0.95$ and hence it is ignored, following previous experimental studies [25]. The properties of all fluids used in the experiments are listed in table I.

The mixed solutions were then used to droplets using a syringe pump, pushing the liquid through a straight stainless-steel needle. By using different needle tips, droplets of varying

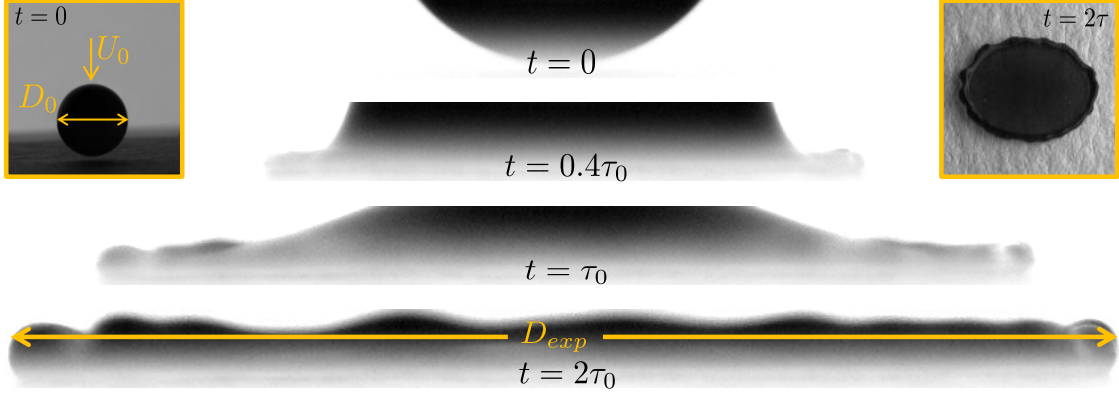


FIG. 1. Successive snapshots of a single droplet impacting on a hydrophobic paper substrate, progressing from impact (top) to maximum spread (bottom). Time is given in terms of the impact timescale, $\tau_0 = D_0/U_0$. Top left: representative frame from the wide-angle camera, used to determine the impact conditions. Top right: representative frame from the isometric-view camera, recording the droplet topology.

initial diameters were obtained, from $D_0 = 2.5$ mm to 4.0 mm. The needle was positioned at different heights above a flat, levelled stage, leading to impact velocities in the range $U_0 = 1.0$ m/s to 2.5 m/s. Two types of substrates were placed on top of the stage: microscope-grade glass (AmScope, BS-72P) and hydrophobic paper sheets (Strathmore, Watercolor, 400 Series), and were replaced after each experiment. The impact of the droplet was recorded by three high-speed cameras simultaneously. A wide-angle view camera (Photron SA5, 5000 fps) was used to measure the droplet diameter and impact speed at the moment of impact, as illustrated in the left-hand inset of figure 1. The spreading event was captured by a narrow-angle view camera (Photron NOVA R-5, 40000 fps); selected subsequent snapshots are presented in figure 1. Owing to the camera's high recording rate and resolution (2048×64 pixels), we were able to determine the maximal spreading diameter and spreading time at high temporal and spatial resolution. In order to minimise the spread of the results and reduce the uncertainty, impact events in which the rim of the droplet exhibited strong irregularity, i.e. splashing and the onset of fingers, were discarded and repeated. The irregularity was identified using a isometric view camera (Photron SA5, 5000 fps) and was limited to within 5% of the equivalent diameter.

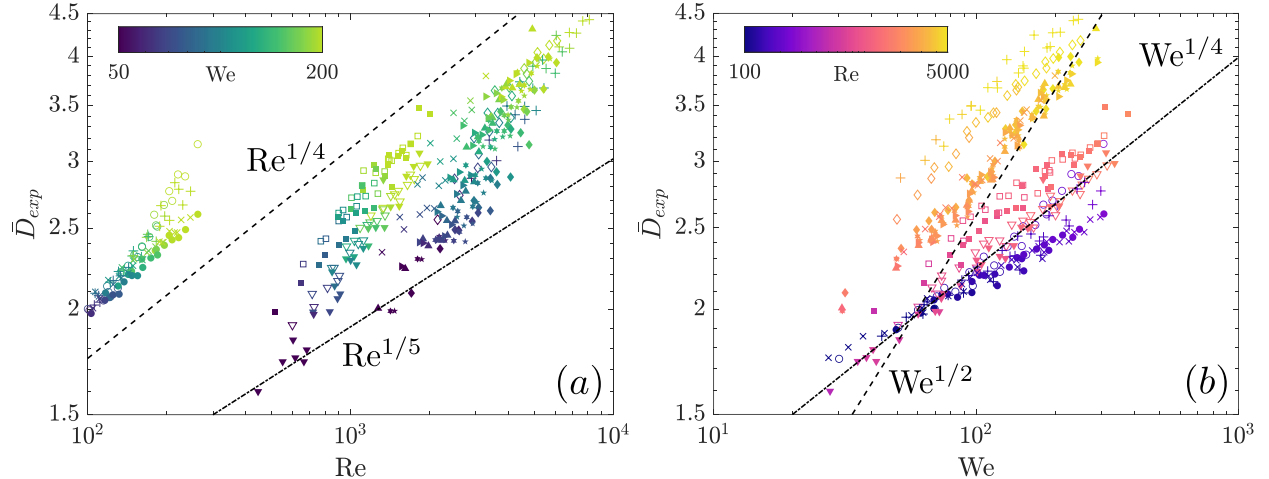


FIG. 2. Measured maximal spreading diameter \bar{D}_{exp} of single droplets of various Newtonian and viscoelastic fluids, detailed in table I. (a) \bar{D}_{exp} versus the impact Reynolds number Re ; dashed and dotted lines indicate $\text{Re}^{1/4}$ and $\text{Re}^{1/5}$ scalings, respectively. Marker colour denotes the impact Weber number We . (b) \bar{D}_{exp} versus the impact Weber number We ; dashed and dotted lines indicate $\text{We}^{1/4}$ and $\text{We}^{1/2}$ scalings, respectively. Marker colour denotes the impact Reynolds number Re .

IV. RESULTS

A representative impact event recorded by the camera array is shown in figure 1. As it impacts the substrate, the droplet flattens and radially expands over the substrate, while its shape evolves into a ‘pizza-like’ shape with a prominent rim [26]. This behaviour is consistent with the present impact conditions ($\text{We} > 30$, $\text{Oh} < 0.1$), for which energy dissipation is predominantly confined to a thin layer near the substrate [9]. For all fluids and substrates used here, the droplets remain attached, and no rebound is observed, although the diameter recedes and oscillates after reaching its maximum; we therefore focus here on the maximal spreading diameter, D_{max} , as it is a strong indicator of the eventual outcome of the impact event.

To evaluate the differences between viscoelastic and Newtonian impacts, we first examine the normalised measured spreading diameter $\bar{D}_{\text{exp}} = D_{\text{exp}}/D_0$ as a function of the impact Reynolds and Weber numbers in figure 2. Within the experimental scatter, no systematic separation between glass and paper substrates is observed, indicating that substrate effects are weak in the present parameter range. This result is consistent with the estimate from equation (7), for which the effect of the contact angle term diminishes when $\text{We} \text{Re}^{-1/2} > |1 - \cos \theta_d|$. Qualitatively, both Newtonian and viscoelastic fluids exhibit the same scaling

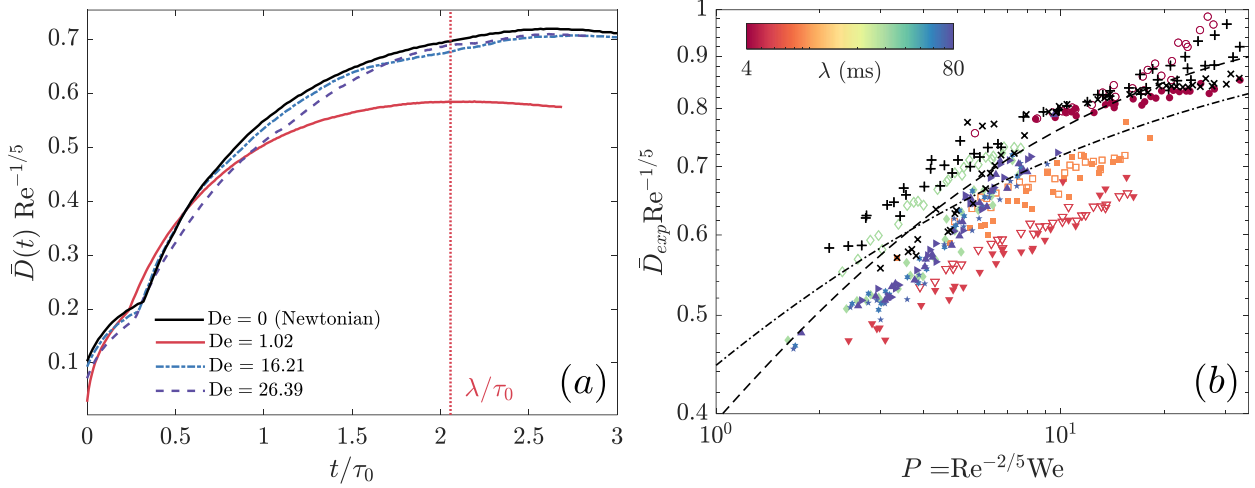


FIG. 3. (a) Temporal evolution of the normalised spreading diameter, $\bar{D}_{\text{exp}} \text{Re}^{-1/5}$, for four representative droplets (0 ppm, 25 ppm, 100 ppm, and 200 ppm of PAAmm) with Deborah numbers 0, 1.02, 16.21, and 26.39, respectively, all at an impact parameter range $P = 6.75 \pm 0.05$. The vertical dashed line marks the dimensionless relaxation time λ/τ_0 for the case $\text{De} = 1.02$; for the other viscoelastic cases, λ/τ_0 lies outside the spreading timescale. (b) Maximal normalised spreading, $\bar{D}_{\text{exp}} \text{Re}^{-1/5}$, versus the impact parameter $P = \text{Re}^{-2/5} \text{We}$ for single impacting droplets of various Newtonian and viscoelastic fluids, detailed in table I. Marker colour indicates the fluid elastic relaxation time λ ; Newtonian fluids with $\lambda \rightarrow 0$ are shown in black. The Padé correlation of Laan *et al.* [11] (dotted) and a second-order fit to the present Newtonian data in equation (8) are shown for comparison.

behaviour, in general agreement with previous models and with the asymptotic behaviour of equation (7). For large We , the scaling with Re tends towards $\bar{D}_{\text{max}} \propto \text{Re}^{1/4}$, as evident in figure 2(a). At the other end of the scaling range, for large Re , a $\text{We}^{1/2}$ scaling emerges in figure 2(b), again consistent with the limits of our model, which supports the view that an energy-balance framework is appropriate for estimating the maximal spreading under our experimental conditions. Overall, the scalings in figure 2 show that viscoelastic droplets obey the same leading-order inertia–capillary asymptotic behaviour as Newtonian droplets. Still, they do not yet isolate the viscoelastic effects.

Let us now consider four cases of impact; in all of them, the impact parameter P lies within a narrow range of $P = 6.75 \pm 0.05$. When considering the rescaled maximal spreading diameter $\bar{D} \text{Re}^{-1/5}$ following Laan *et al.* [11], one would expect that, if no viscoelastic effects were to emerge, all of the spreading events would unfold in the same manner. When the diameter is tracked over time, one observes that the evolution is essentially the same. As expected, each impact begins with a short contact phase ($t/\tau_0 \lesssim 0.5$) during which the

droplet first hits the substrate and flattens. Once the contact diameter exceeds the initial diameter, the droplet spreads approximately as $D \propto \sqrt{t}$, consistent with the canonical inertial–capillary regime reported in previous experimental and numerical studies [6, 7].

Here, a significant difference between the cases is observed: when the Deborah number is around unity, spreading is significantly hindered compared with the Newtonian case. The maximal (rescaled) diameter is significantly lower, and the spreading time, defined as the time between initial contact and maximal spreading, is shorter. Interestingly, and rather unintuitively but supported by our simplified model, the other viscoelastic droplet does not exhibit a substantial deviation from the Newtonian dynamics. Although they have higher polymer concentration and thus a higher Deborah number, both their diameter evolution and spreading time remain similar to those in the Newtonian case.

Figure 3(b) extends this analysis using the rescaled diameter representation to highlight the influence of viscoelasticity. The Newtonian data (black symbols) collapse onto a single, well-defined branch, whereas several viscoelastic fluids deviate from this trend. In particular, two fluids with relaxation times in the range $\lambda = 6\text{--}10\text{ ms}$ exhibit the most significant deviations from the spreading of Newtonian droplets across all impact conditions. However, as we increase the elastic relaxation time, the spreading behaviour gradually reverts towards the Newtonian case; the deviation from Newtonian behaviour is therefore a non-monotonic function of the elastic relaxation time λ .

To quantify the extent of this deviation and its dependence on the fluid properties and impact conditions, we first require a reliable benchmark correlation for the maximal spreading of Newtonian droplets under our experimental conditions. We therefore compare the Newtonian data to the Padé approximant proposed by Laan *et al.* [11], given in equation (1); however, it is found to underestimate the rescaled maximal spreading in our parameter range. We then consider a second-order Padé approximant, similar in form to that proposed by Mobaseri *et al.* [14],

$$\bar{D}_{\text{cor}} \text{Re}^{-1/5} = \frac{0.37P + \sqrt{P}}{0.37P + \sqrt{P} + 2.1}. \quad (8)$$

This higher-order approximant captures the Newtonian data reasonably well for $P \gtrsim 10$, but still tends to underestimate the measured spreading.

Finally, we consider the higher-order correlation suggested by Sanjay and Lohse [9] for

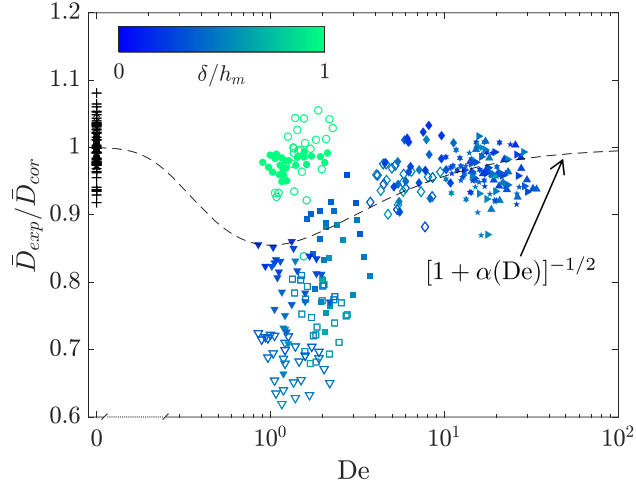


FIG. 4. Deviation of the measured spreading diameter from the expected value at given impact conditions, $\bar{D}_{\text{exp}}/\bar{D}_{\text{cor}}$, as a function of De . For reference, all the Newtonian data are plotted at $\text{De} = 0$. Marker colour indicates the ratio of viscous boundary-layer thickness to maximal film thickness, δ/h_m ; the dashed line illustrates the function $f(\text{De}) = (1 + \alpha)^{-1/2}$.

impacts in the present We–Oh range, which can be written as

$$\bar{D}_{\text{cor}} = \sqrt{\alpha_0 + \alpha_1 \text{We} \left(1 - \frac{b_0 + b_1 \text{Re}^{1/10} + b_2 \text{Re}^{-1/10} \sqrt{\text{We}}}{\sqrt{\text{Re}}} \right)}, \quad (9)$$

with α_0 , α_1 , b_0 , b_1 and b_2 empirical constants fitted using the spreading diameters recorded for Newtonian fluids. This correlation proves to be the most accurate for our Newtonian data, estimating the maximal spreading diameter within approximately 10% across the tested impact conditions.

Using equation (9), we can now directly compare the measured maximal spreading to the Newtonian prediction at the same impact conditions by calculating the ratio $\bar{D}_{\text{exp}}/\bar{D}_{\text{cor}}$. This ratio is plotted in figure 4 as a function of the Deborah number De . A clear trend emerges: the spreading of viscoelastic drops is reduced relative to the Newtonian correlation. The reduction in maximal spreading diameter is found to be up to 40%, and this reduction is significantly larger than the experimental scatter, as can be seen by comparison with the Newtonian data, which collapse near $\bar{D}_{\text{exp}}/\bar{D}_{\text{cor}} \approx 1 \pm 0.1$ at $\text{De} = 0$. Moreover, our results suggest that the most significant suppression of spreading occurs around $\text{De} \approx 1$, in good agreement with the model prediction of equation (7), represented by the dashed curve. However, one set of measurements lies systematically above the main viscoelastic branch;

these impacts correspond to the most viscous fluid in our set. For this fluid, the viscous boundary-layer thickness $\delta \approx \sqrt{\nu\tau_f}$ is estimated to exceed the measured droplet thickness at the point of maximal spread h_m ($\delta/h_m \gtrsim 1$), as highlighted by the colour scale. Hence, one may argue that for this set of experiments, the viscous dissipation becomes dominant and partially masks the elastic effect encapsulated by the parameter $\alpha(\text{De})$. The elastic effects also vanish when the Deborah number increases to $\text{De} \geq 10$. The maximal spreading diameter in this region does not deviate from Newtonian behaviour, as the measurements fall within the expected experimental uncertainty. This observation is consistent with previous studies [19], which reported Newtonian-like spreading in this regime.

V. CONCLUSIONS

The effect of viscoelasticity on droplet spreading upon impact remains difficult to isolate. To clarify the underlying physical mechanisms governing the spreading dynamics, we proposed a simplified theoretical model, supported by impact experiments, to quantify how fluid elasticity modifies the maximal spreading of impacting droplets and to identify the parameters governing departures from Newtonian behaviour. Experiments were performed using dilute polyacrylamide (PAAmm) solutions with similar viscosity and surface tension but varying relaxation time, impacting on glass and hydrophobic paper substrates, with the spreading dynamics recorded by a three-camera high-speed imaging system.

We find that viscoelastic droplets follow the same leading-order inertia–capillary asymptotic scalings as Newtonian fluids. However, when the maximal spreading diameter of viscoelastic droplets is normalised and compared to Newtonian predictions at the same impact conditions, deviations emerge that can be attributed to fluid elasticity. These deviations are non-monotonic in the Deborah number and attain their maximum when the elastic relaxation time is comparable to the spreading timescale, i.e. $\text{De} \approx 1$.

These results support the general prediction of our introduced model: an extension of classical energy balance that incorporates viscoelastic effects through a single correction factor, $\alpha(\text{De})$. This model captures the observed reduction in maximal spreading and predicts both the location and magnitude of the most substantial viscoelastic effects. When viscous dissipation dominates the impact, as indicated by a viscous boundary-layer thickness exceeding the spreading lamella thickness, elastic effects are masked, and the spreading

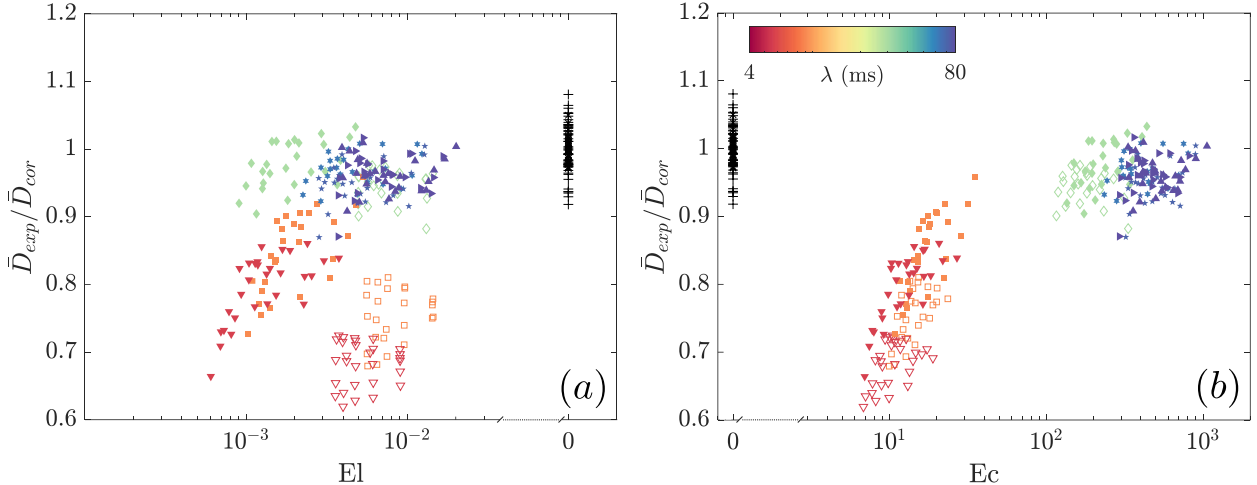


FIG. 5. Deviation of the measured maximal spreading from the Newtonian correlation, $\bar{D}_{\text{exp}}/\bar{D}_{\text{cor}}$, plotted against viscoelastic control parameters. Marker colour indicates the fluid relaxation time λ . (a) $\bar{D}_{\text{exp}}/\bar{D}_{\text{cor}}$ as a function of the elasticity number $\text{El} = \text{De}/\text{Re}$. (b) $\bar{D}_{\text{exp}}/\bar{D}_{\text{cor}}$ as a function of the elasto-capillary number $\text{Ec} = \text{DeRe}/\text{We}$.

reverts towards Newtonian behaviour. That is, increasing polymer concentration does not necessarily increase the deviation from Newtonian behaviour; instead, measurable viscoelastic effects arise only within a narrow window where the elastic and spreading timescales are comparable. The framework presented here provides a direct route for incorporating viscoelasticity into well-established droplet-impact correlations and offers a basis for extending current impact models beyond purely Newtonian fluids.

ACKNOWLEDGMENTS

We thank L. Kramer for her help in conducting initial experiments. O.A. was supported by a Fulbright Postdoctoral Fellowship. D.W. was partially supported by a UTRA Fellowship. R.Z. acknowledges the funding from the Petroleum Research Fund (Grant Number 66922-ND9).

Appendix A: Dimensionless elasticity numbers

To further delineate the region in which viscoelasticity affects the maximal spreading, we examine the deviation from the Newtonian correlation, $\bar{D}_{\text{exp}}/\bar{D}_{\text{cor}}$, in terms of the elasticity and elasto-capillary numbers, as shown in figure 5. Figure 5(a) shows $\bar{D}_{\text{exp}}/\bar{D}_{\text{cor}}$ plotted

against the elasticity number $\text{El} = \text{De}/\text{Re}$; over the examined range, $\text{El} \sim 10^{-3}\text{--}10^{-2}$, the data exhibit substantial scatter and no clear trend, indicating that El alone does not parameterise the viscoelastic correction under the present impact conditions.

In contrast, when the same data are plotted as a function of the elasto-capillary number $\text{Ec} = \text{De}\text{Re}/\text{We}$ in figure 5(b), a clear separation of scales emerges. For high Ec values ($10^2\text{--}10^3$), no significant viscoelastic effects are observed; however, as Ec decreases towards order 10^2 , the ratio $\bar{D}_{\text{exp}}/\bar{D}_{\text{cor}}$ decreases, indicating a growing reduction of the maximal spread relative to the Newtonian prediction. These trends suggest that measurable deviations in maximal spreading arise when elastic stresses become comparable to capillary stresses in the spreading lamella. Although not attainable in the current experimental setup, one might postulate, based on the observed trend, that elastic effects peak at $\text{Ec} \approx 1$.

[1] S. Chandra and C. T. Avedisian, *Proceedings of the Royal Society of London. Series A: Mathematical and Physical Sciences* **432**, 13 (1997), publisher: Royal Society.

[2] D. Bonn, J. Eggers, J. Indekeu, J. Meunier, and E. Rolley, *Reviews of Modern Physics* **81**, 739 (2009), publisher: American Physical Society.

[3] D. Lohse, *Annual Review of Fluid Mechanics* **54**, 349 (2022), publisher: Annual Reviews.

[4] A. L. Yarin and D. A. Weiss, *Journal of Fluid Mechanics* **283**, 141 (1995).

[5] R. Rioboo, M. Marengo, and C. Tropea, *Experiments in Fluids* **33**, 112 (2002).

[6] J. Eggers, M. A. Fontelos, C. Josserand, and S. Zaleski, *Physics of Fluids* **22**, 062101 (2010).

[7] M. Pasandideh-Fard, Y. M. Qiao, S. Chandra, and J. Mostaghimi, *Physics of Fluids* **8**, 650 (1996).

[8] Y. Ma and H. Huang, *Physical Review Fluids* **9**, 113601 (2024), publisher: American Physical Society.

[9] V. Sanjay and D. Lohse, *Physical Review Letters* **134**, 104003 (2025), publisher: American Physical Society.

[10] L. Liu, G. Cai, W. Wang, B. He, and P. A. Tsai, *Journal of Fluid Mechanics* **1018**, A42 (2025).

[11] N. Laan, K. G. De Bruin, D. Bartolo, C. Josserand, and D. Bonn, *Physical Review Applied* **2**, 044018 (2014).

[12] S. M. An and S. Y. Lee, *Experimental Thermal and Fluid Science* **38**, 140 (2012).

- [13] F. Boyer, E. Sandoval-Nava, J. H. Snoeijer, J. F. Dijksman, and D. Lohse, *Physical Review Fluids* **1**, 013901 (2016).
- [14] A. Mobaseri, S. Kumar, and X. Cheng, *Proceedings of the National Academy of Sciences* **122**, e2500163122 (2025).
- [15] D. Bonn and J. Meunier, *Physical Review Letters* **79**, 2662 (1997).
- [16] J. Dinic and V. Sharma, *Proceedings of the National Academy of Sciences* **116**, 8766 (2019), publisher: *Proceedings of the National Academy of Sciences*.
- [17] J. Song, N. Holten-Andersen, and G. H. McKinley, *Soft Matter* **19**, 7885 (2023).
- [18] S. I. Tamim and J. B. Bostwick, *npj Microgravity* **7**, 42 (2021).
- [19] B. Gorin, G. Di Mauro, D. Bonn, and H. Kellay, *Langmuir* **38**, 2608 (2022).
- [20] V. Bergeron, D. Bonn, J. Y. Martin, and L. Vovelle, *Nature* **405**, 772 (2000).
- [21] D. Bartolo, A. Boudaoud, G. Narcy, and D. Bonn, *Physical Review Letters* **99**, 174502 (2007).
- [22] C. Clanet, C. Béguin, D. Richard, and D. Quéré, *Journal of Fluid Mechanics* **517**, 199 (2004).
- [23] J. Dinic, Y. Zhang, L. N. Jimenez, and V. Sharma, *ACS Macro Letters* **4**, 804 (2015).
- [24] M. Ravisankar and R. Zenit, *Physical Review Letters* **135**, 024003 (2025).
- [25] S. Yamani, B. Keshavarz, Y. Raj, T. A. Zaki, G. H. McKinley, and I. Bischofberger, *Physical Review Letters* **127**, 074501 (2021).
- [26] S. Wildeman, C. W. Visser, C. Sun, and D. Lohse, *Journal of Fluid Mechanics* **805**, 636 (2016).